RESEARCH ARTICLE

AMERICAN JOURNAL OF BOTANY

Vascular development in very young conifer seedlings: Theoretical hydraulic capacities and potential resistance to embolism[1]

Megan L. Miller[2] and Daniel M. Johnson

PREMISE OF THE STUDY: Conifers have the highest rates of mortality during their first year, often attributed to water stress; yet, this tree life stage is the least studied in terms of hydraulic properties. Previous work has revealed correlations between xylem anatomy to both hydraulic transport capacity and resistance to hydraulic dysfunction. In this study, we compared xylem anatomical and plant functional traits of *Pseudotsuga menziesii*, *Larix occidentalis*, and *Pinus ponderosa* seedlings over the first 10 wk of growth to evaluate potential maximum hydraulic capabilities and resistance to drought-induced embolism. We hypothesized that, based on key functional traits of the xylem, predicted xylem embolism resistance of the species will reflect their previously determined drought tolerances with *L. occidentalis*, *P. menziesii*, and *P. ponderosa* in order of least to most embolism-resistant xylem.

METHODS: Xylem and pit anatomical characteristics and additional hydraulic-related functional traits were compared at five times during the first 10 wk of growth using confocal laser scanning microscopy (CLSM).

KEY RESULTS: Based on thickness to span ratio, torus to pit aperture overlap, and torus thickness, primary xylem appeared to be not only more hydraulically conductive but also less embolism-resistant than secondary xylem. By week 10, *P. menziesii* was predicted to have the most embolism-resistant xylem followed by *P. ponderosa* and *L. occidentalis*.

CONCLUSIONS: Theoretical measurements suggest that hydraulic transport capacities and vulnerability to embolism varied for each species over the first 10 wk of growth; thus, the timing of germination and onset of limited soil moisture is critical for growth and survival of seedlings.

KEY WORDS bordered pits; confocal laser scanning microscopy (CLSM); Douglas-fir; functional anatomy; Pinaceae; ponderosa pine; primary growth; secondary growth; torus-margo; western larch

The first year of life is a perilous stage in tree life history because first-year seedlings have the highest rates of mortality (e.g., Burns and Honkala, 1990). Yet, seedling survival is critical for maintaining natural forest regeneration and facilitating species migrations, especially considering current climate change predictions. Despite vast amounts of research on woody plant anatomy and physiology, there remains a paucity of research on first-year conifer seedling functional anatomy, water-related functional traits, and in vitro hydraulic variables (Johnson et al., 2011; Kerr et al., 2015; Reinhardt et al., 2015). A functional trait refers to any plant characteristic that may influence how the plant interacts with other plants and with the environment as well as impacts on recruitment and fitness (Reich et al., 2003; Pérez-Harguindeguy et al., 2013). Key plant functional traits vary widely depending upon the question of interest and can be used to make inferences about plant ecophysiology (Santiago et al., 2004; Lambers et al., 2008; Pérez-Harguindeguy et al., 2013).

Previous research on saplings and mature trees identified several key anatomical and functional traits that correlate with in vitro hydraulic variables. One of the most commonly reported hydraulic variables is the water potential at which 50% of hydraulic conductivity is lost (P_{50}) (see Gleason et al., 2016 and references therein). This value is often used as a proxy for drought tolerance whereby a more negative P_{50} means increased embolism resistance and thus greater drought tolerance (Martínez-Vilalta et al., 2004). In gymnosperms, functional traits that have been shown to correlate with P_{50} include tracheid lumen diameter (D_l) (Sperry et al., 2006, but see

[1] Manuscript received 1 May 2017; revision accepted 5 June 2017.
875 Perimeter Drive MS 1133, College of Natural Resources, University of Idaho, Moscow, Idaho 83844 USA
[2] Author for correspondence (e-mail: meganlmiller.30@gmail.com)
https://doi.org/10.3732/ajb.1700161

Pittermann et al., 2010), hydraulic diameter (D_h) (Corcuera et al., 2012; Sterck et al., 2012; Bouche et al., 2014; but also see Tyree and Zimmermann, 2002), tracheid density/wood density (Hacke and Sperry, 2001; Pittermann et al., 2006b; Sterck et al., 2012; Ogasa et al., 2013), thickness to span ratio (T_w/D_t; i.e., wall thickness to tracheid diameter) (Hacke and Sperry, 2001; Hacke et al., 2001; Pittermann et al., 2006b; Domec et al., 2009; Sterck et al., 2012; Bouche et al., 2014), and torus to pit aperture overlap (TPO) (Delzon et al., 2010; Pittermann et al., 2010; Bouche et al., 2014). In addition to these characteristics, other functional traits, such as xylem specific conductivity, leaf specific conductivity, and leaf area to sapwood area, correspond to adaptations for maintaining hydraulic continuity, resistance to embolism, drought responses, transpiration, and carbon investment priorities (Tyree and Ewers, 1991; Tyree and Zimmermann, 2002; Santiago et al., 2004; Lambers et al., 2008; Melcher et al., 2012; Pérez-Harguindeguy et al., 2013).

It is also currently unknown whether the mechanisms for mediating drought-induced mortality and hydraulic dysfunction are similar between seedling, sapling, and mature stages of life (Anderegg and Anderegg, 2013; Clark et al., 2016); young seedlings may not have the necessary anatomical structures to resist embolism nor the carbohydrate stores and hydraulic capacitance to survive long-term stomatal closure during prolonged drought episodes (Kitajima and Myers, 2008; Lambers et al., 2008; Johnson et al., 2011; Reinhardt et al., 2015). Additionally, very young seedlings may lack additional factors that enhance resistance to drought-induced hydraulic dysfunction such as thickened leaf cuticle (i.e., in cotyledons, primary leaves, and early secondary leaves), regulation of stomatal conductance and water-use efficiencies, rooting depths, allometric adjustments, and extensive mycorrhizal associations (Simonin et al., 2006; Facelli, 2008; Horton and van der Heijden, 2008; Lambers et al., 2008; Johnson et al., 2011; Schall et al., 2012; Clark et al., 2016). Thus, seedlings may be more reliant on internal anatomical structures (i.e., xylem anatomy) for maintenance of hydraulic transport and associated resistance to drought-induced hydraulic dysfunction.

Our objective was to determine the patterns of seedling growth and vascular development and to specifically assess (1) tracheid size distributions, (2) contributions of primary and secondary xylem to theoretical conductivities, (3) traits correlated to embolism resistance (i.e., P_{50}), and (4) internal mechanisms for reducing hydraulic dysfunction during drought. We analyzed vascular development and specific functional traits associated with plant-water relations (Table 1) at 2, 3, 4, 6, and 10 wk after seeding in three native conifers of the inland Northwest of the United States: *Pinus ponderosa* Dougl. ex Laws, *Pseudotsuga menziesii* (Mirb.) Franco, and *Larix occidentalis* Nutt. We hypothesized that key anatomical and functional traits represent a spectrum that reflects in situ drought tolerances, whereby *L. occidentalis*, *P. menziesii*, and *P. ponderosa* are in order of least to most resistant to embolism, commensurate with published relative drought tolerances (Piñol and Sala, 2000).

TABLE 1. Descriptions, abbreviations, and units of anatomical and functional characteristics evaluated for *Larix occidentalis*, *Pseudotsuga menziesii*, and *Pinus ponderosa* seedlings.

Abbreviations	Explanation	Units
Anatomical features		
T_w	Tracheid double wall thickness	μm
D_{pa}	Pit aperture diameter	μm
D_m	Membrane diameter	μm
D_{tor}	Torus diameter	μm
T_t	Torus thickness	μm
D_t	Span; tracheid lumen diameter	μm
A_t	Tracheid lumen area	μm^2
A_L	Leaf Area	m^2
A_s or D_s	Cross-sectional stem area (or diameter)	mm^2 (mm)
A_x or D_x	Cross-sectional xylem area (or diameter) (includes pith)	mm^2 (mm)
A_{tx}	Actual measured total xylem area (excludes pith)	mm^2
A_{sx}	Xylem sampled area	mm^2
A_{sfx}	Functional xylem area within A_{sx}	mm^2
A_{tfx}	Calculated total functional xylem area	mm^2
Functional traits		
$K_{s(t)}$	Theoretical xylem specific conductivity	$kg \cdot m^{-1} \cdot s^{-1} \cdot MPa^{-1}$
$K_{h(t)}$	Theoretical hydraulic conductance	$kg \cdot m \cdot s^{-1} \cdot MPa^{-1}$
$K_{L(t)}$	Theoretical leaf specific conductivity	$kg \cdot m^{-1} \cdot s^{-1} \cdot MPa^{-1}$
TPO	Torus to pit aperture overlap	—
T_w/D_t	Thickness to span ratio	—
$A_L:A_{tfx}$	Leaf area to functional xylem area	—
$A_{tfx}:A_x$	Functional tracheid lumen fraction	—
P_{50}	Water potential at which 50% of maximum hydraulic conductivity is lost	MPa

MATERIALS AND METHODS

Plant materials and growing conditions—Seeds from all species were germinated in early mid April 2015 at the University of Idaho's Franklin H. Pitkin Forest Nursery in Moscow, Idaho, United States (46°43′N, 116°59′W). Seeds were sourced from the local region (University of Idaho's Experimental Forest) to minimize geographical differences in intraspecific characteristics. Seeds were sown in 4–5 trays of 96 conical cells (3.8 × 21.0 cm, top diameter × length) (SC10R; Stuewe & Sons, Tangent, Oregon, USA) per species containing a commercial potting mix (Metro-Mix Custom Blend; Sun Gro Horticulture, Agawam, Massachusetts, USA) consisting of 40–50% sphagnum peat moss, vermiculite, and aged fine bark.

All trays were watered according to procedures discussed by Landis (1989a) and were fertilized weekly using a locally procured MiracleGro Fertilizer (NPK 24:8:16) targeted at a nitrogen application of 100 ppm (Landis, 1989b). Additional phosphoric acid (H_3PO_4) was used to further acidify the water or aqueous fertilizer. Trays were randomized weekly within the greenhouse benches to minimize microclimate variations and edge effects. The greenhouse bay was computer-automated climate controlled with 15-min monitoring intervals of temperature and relative humidity. Supplemental lighting extended the photoperiod to 14 h per day for the length of the growing season.

Confocal laser scanning microscopy—Confocal laser scanning microcopy (CLSM) utilizes multiple laser beams of differing wavelengths and a pinhole light aperture to optically image specimens in the *x*, *y*, and *z* directions, creating an optical three-dimensional (3D) image (Ruzin, 1999). It has been well established for analyzing plant cellular and anatomical characteristics (for a review, see Hepler and Gunning, 1998). During growth, at least five seedlings were randomly collected from each species at each time period. They were collected from the greenhouse intact, wrapped in wet paper

towels, bagged, and immediately transported to the laboratory. Growing media was removed, and the samples were placed in FAA (95% ethanol–acetic acid–37% formaldehyde–water; 50:5:10:35 v/v) (Ruzin, 1999), degassed under a partial vacuum overnight, and retained in FAA until imaging. For the very young, delicate samples, the entire seedling (root, stem, crown) was placed into the fixative. For older or larger samples, the seedlings were severed either slightly below the root collar or at the crown (or both) just before fixation. In this case, roots and crowns were retained and stored separately in FAA.

Before imaging, the fixed specimens were rinsed three times in deionized water at 15 min per rinse. If not previously excised, the root and crown were removed from the main stem, which was then transected at approximately the midstem point, 0.09 ± 0.02 cm (SE), 1.4 ± 0.06 cm, and 2.1 ± 0.03 cm for *L. occidentalis*, *P. menziesii*, and *P. ponderosa*, respectively, and the crowns were retained for leaf area measurements (see below). The upper stem segments were processed according to Kitin et al. (2003). Briefly, the stem segments were placed in 0.01% or 0.06% safranin O under vacuum for 30 min, rinsed in deionized water to remove excess stain, dehydrated then rehydrated in stepped acetone solutions (0%, 25%, 50%, 75%, 100%) at 15 min per interval. The specimens were finally cleared in stepped glycerol concentrations (25%, 50%, 75%, and 100%) and stored in 100% glycerol. Immediately before imaging, the stem segments were hand-sectioned from the midstem end using a double-edged razor blade and mounted in glycerol on a microscope slide with a cover slip; average section thicknesses were 80 ± 4 μm (SD).

Sections were optically scanned using an Olympus Fluoview 1000 (FV-1000) confocal microscope (Olympus America, Center Valley, Pennsylvania, USA) with excitation of three laser lines at 405, 488, and 559 nm and three emission filters (SDM490, SDM560 and BF, respectively). The ranges of these emission filters were 425–475 nm, 500–545 nm, and 575–675 nm, respectively, but each range could be further restricted to better distinguish specific anatomical characteristics of interest (Bond et al., 2008; Sant'Anna et al., 2013). Narrowing the range of SDM560 and BF filters to 520–540 nm and 575–620 nm, respectively, often reduced background cellular noise, making the cell walls easier to view. Overlaying the three different images, each produced from a single excitation laser (Fig. 1A–C), into a composite image (Fig. 1D) at three magnifications (10×, 20×, and 60×) provided details for distinguishing anatomical characteristics and facilitated anatomical measurements (Fig. 2A). Due to differing safranin O concentrations, species, specimen distance from transected end, and changing tissue quantity and chemical composition (i.e., lignin to cellulose ratios) during growth, CLSM operational settings including laser power, aperture settings, *Z*-step (i.e., optical scanning depth), and emission filter ranges had to be continuously modified as necessary. Additionally, based on system settings, postimaging nonlinear color adjustments were used when necessary, especially to distinguish cell cytoplasm. The color adjustments and specific operational parameters used for all figures are in Appendix S1 (see Supplemental Data with this article).

Anatomical measurements—A total of 79 seedlings, four to seven seedlings per species per time period, were measured for anatomical properties; 75 of these were measured for functional traits because two seedlings were not suitable for in-depth xylem image analysis and two image files could not be retrieved after imaging. Week 10 was chosen as the end point of anatomical analyses because we assumed from this point there would be no additional major anatomical development besides the radial expansion of secondary xylem and development of the cork tissue, which was outside the scope of this study.

All tracheid anatomical features were measured on mature primary and secondary xylem, where mature tracheids were defined by the lack of live cell contents as viewed with confocal microscopy (Fig. 2B); all mature tracheids were assumed to be functional in stem water transport. Stem cross-sectional diameter (D_s), xylem cross-sectional diameter (D_x), and total xylem area (A_{tx}) per stem were measured utilizing the 10× and 20× CLSM images; two linear measurements of D_s and D_x were averaged per stem and used to calculate stem and xylem cross-sectional areas (A_s and A_x, respectively). A sample area (A_{sx}) was randomly delineated per stem, approximately wedge-shaped, that included entire radial files of xylem from the pith to vascular cambium. Functional xylem area was measured directly (60× magnification) within this sample area (A_{sfx}) and extrapolated to estimate total stem functional xylem area per stem (A_{tfx}):

$$A_{\mathrm{tfx}} = \left(\frac{A_{\mathrm{sfx}}}{A_{\mathrm{sx}}}\right) A_{\mathrm{tx}}.$$

When the sample area size exceeded that of the 60× field of view (211.97 × 211.97 μm), several scans were taken to encompass the entire sample area and subsequently stitched together using the ImageJ "pairwise stitching" plugin (Preibisch et al., 2009). Tracheid lumen area (A_t) for all mature tracheids within the sample area were measured and converted into circle equivalent lumen diameters (D_t) (i.e., span). A randomized subset of an average of 31 ± 12.05 (SD) tracheids within each sample area were selected for wall thickness (T_w) measurements, which consisted of a linear measurement of the double wall thickness between the selected tracheid and at least two adjacent functional tracheids (Sperry et al., 2006; Bouche et al., 2014) (Fig. 3).

Bordered pit anatomical characteristics including pit aperture diameter (D_{pa}), membrane diameter (D_m) (assumed to be the inner diameter of the pit), torus diameter (D_{tor}) and approximate torus thickness (T_t), were measured in primary and secondary xylem within the 60× field of view or within the total xylem area if xylem area was smaller than the field of view (Fig. 3). Torus characteristics are typically measured using SEM or TEM (see Jansen et al., 2008 and references therein); however, to our knowledge, there has not been a direct comparison between CLSM and SEM/TEM. Estimated values of torus thickness based on Jansen et al. (2012) and Schulte et al. (2015) indicate that the minimum resolution of CLSM at 60× (0.207 μm/pixel) is adequate enough to approximate torus anatomical variables and establish inter- and intraspecific comparisons. The 3D imaging capacity of CLSM also provided the additional benefit of ensuring that cross sections were measured at the pit center, assumed to be either the thickest part of the torus or the largest membrane diameter. Bordered pit characteristics were only measured when the adjoining two tracheids were mature with no evidence of cell plasma within the pit space.

Leaf area was measured on a random subset of 5 ± 1.2 (SD) crowns per species per time period. Cotyledons were included in leaf area if they were still attached to the crown stem. All leaves per crown were removed, placed under clear Plexiglass to flatten needles, and photographed with a ruler for scale. All anatomical

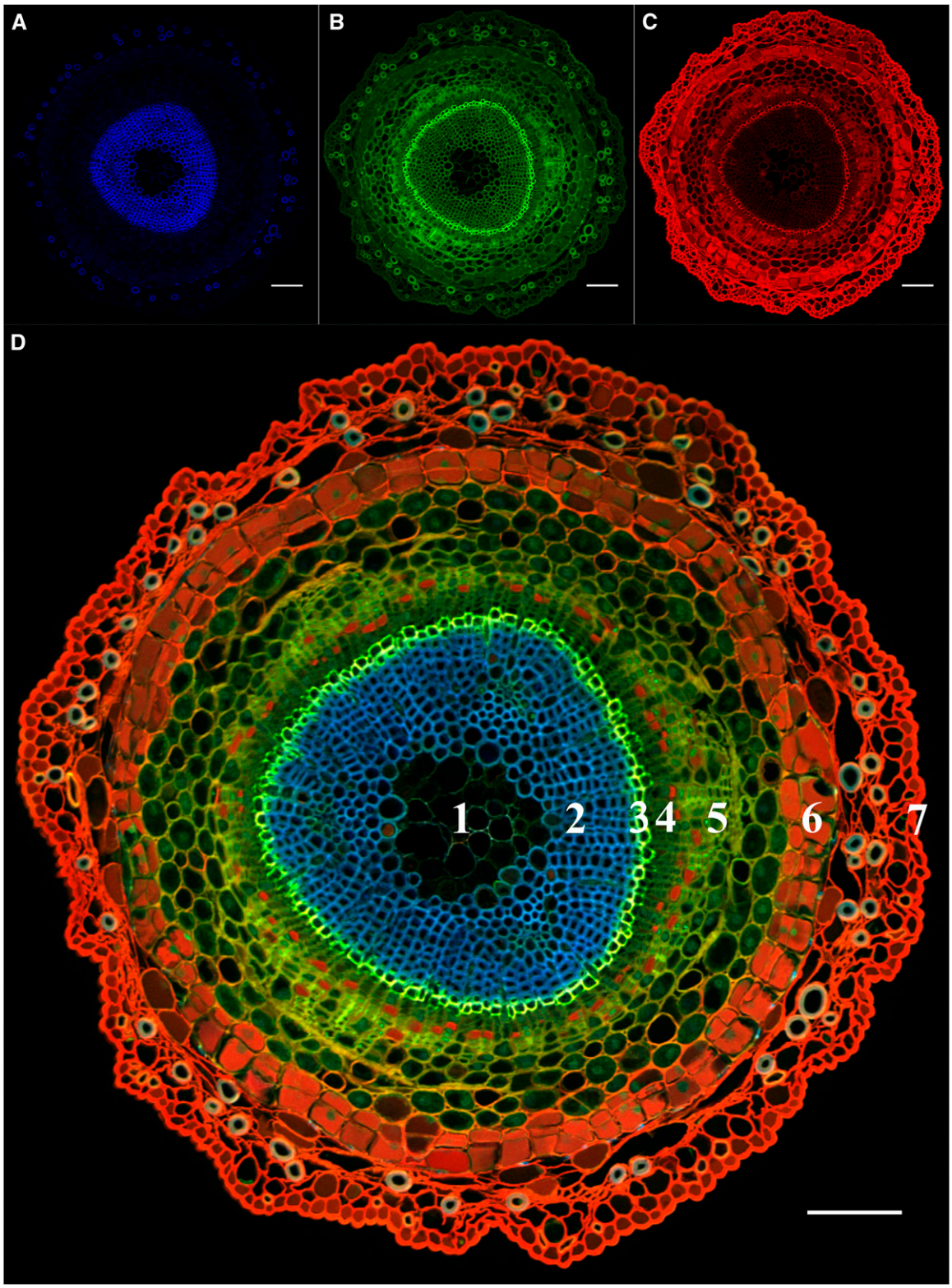

FIGURE 1 Composite confocal laser scanning microscopy (CLSM) image of 4-wk-old *Pseudotsuga menziesii* stained with safranin O. The three confocal laser wavebands (A) 405 nm, (B) 488 nm, and (C) 559 nm excite overlapping and individual anatomical and cellular components based on cellular and chemical properties. Each waveband is associated with a false color for viewing (blue, green, and red, respectively). The composite image (D) illustrates how the three wavelengths can produce images very clearly delimiting stem anatomy: 1. pith, 2. mature xylem, 3. differentiating xylem, 4. vascular cambium, 5. phloem, 6. cork cambium, and 7. epidermis. The differences in color of the cell walls between differentiating xylem and mature xylem are due to differences in lignin/cellulose content. Bar = 100 µm. CLSM system settings and image postprocessing parameters are available in Appendix S1.

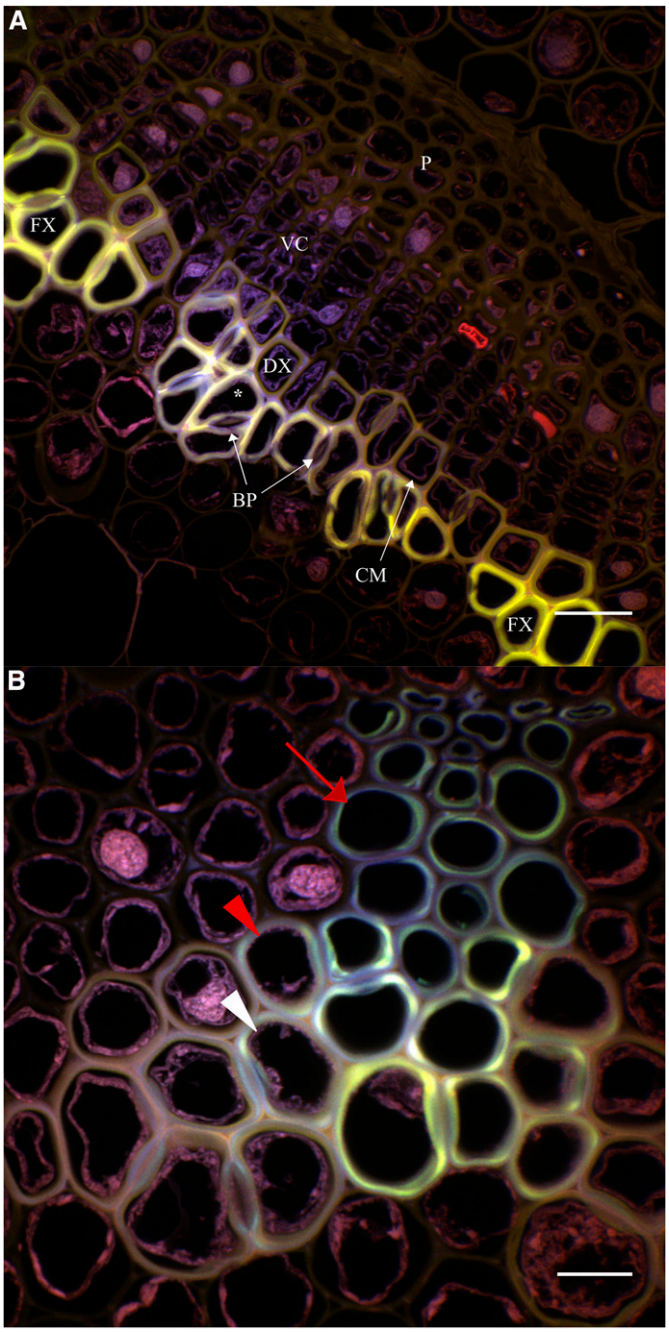

FIGURE 2 Vascular tissue of (A) 3-wk-old *Pinus ponderosa* and (B) 2-wk-old *P. ponderosa*. (A) Functional xylem (FX), differentiating xylem (DX), tracheid undergoing programmed cell death, (*), vascular cambium (VC), plasmolyzed cell membrane (CM), bordered pits with visible torus (BP), phloem (P), and cell wall S1 to S3 cell layers (not shown). (B) Differentiating primary xylem. Live cell membranes and nuclei (pink) are visible with safranin O staining, enabling identification of live xylem undergoing differentiating (white arrowhead), tracheids undergoing programmed cell death with remnant cell wall contents (red arrowhead) and a mature functional tracheid (red arrow). Protoxylem at top right of image is undergoing physical deformation. Note the differences in cell wall color between older, mature xylem (blue) and live xylem (orange/yellow). Bar = (A) 25 µm; (B) = 15 µm. CLSM system settings and image postprocessing parameters are available in Appendix S1.

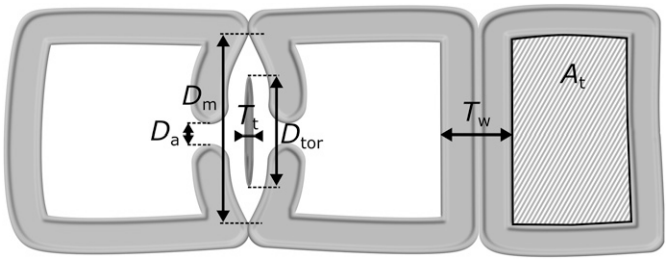

FIGURE 3 Diagrammatic transverse view of three adjacent tracheids and associated measurements. A_t = tracheid lumen area, D_a = pit aperture diameter, D_m = membrane diameter, D_{tor} = torus diameter, T_t = torus thickness, T_w = double cell wall thickness between two adjacent tracheids.

variables were measured utilizing Fiji/ImageJ (Schindelin et al., 2012; W. S. Rasband, ImageJ, U. S. National Institutes of Health, Bethesda, Maryland, USA, imagej.nih.gov/ij/, 1997–2014).

Functional properties—Theoretical values for hydraulic conductance $K_{h(t)}$, xylem specific hydraulic conductivity $K_{s(t)}$ and leaf specific conductivity $K_{L(t)}$ were calculated. The specific conductivities illustrate the maximum theoretical conductivity per species, allowing for a comparison of conducting efficiency between each species at each time period. Theoretical xylem specific conductivity $K_{s(t)}$ per stem is based on average tracheid lumen diameter and calculated from the Hagen–Poiseuille equation (Tyree and Ewers, 1991; Santiago et al., 2004) as:

$$K_{s(t)} = \frac{\pi\rho}{128\eta A_{tfx}} \sum_{i=1}^{n} D_{ti}^4,$$

where

$$\sum_{i=1}^{n} D_{ti}^4 = \text{sampled} \sum_{i=1}^{n} D_{ti}^4 \left(\frac{A_{tfx}}{A_{tx}} \right),$$

D_{ti} are the individual tracheid lumen diameters, i, to the fourth power and summed for all tracheids, n, $K_{s(t)}$ is the xylem specific conductivity ($kg \cdot m^{-1} \cdot MPa^{-1} \cdot s^{-1}$), ρ is the density of water ($kg \cdot m^{-1}$), and η is the dynamic viscosity of water (MPa) at 20°C, and other symbols are as described previously. Stem conductance $K_{h(t)}$ was estimated by multiplying $K_{s(t)}$ by A_{tfx} (Tyree and Ewers, 1991), and theoretical leaf specific conductivity $K_{L(t)}$ was estimated by dividing $K_{h(t)}$ by the leaf area A_L distal to stem measurement (Tyree and Zimmermann, 2002); in this case, leaf area measurements consisted of entire seedling crowns. Thickness to span ratios (T_w/D_t) were calculated for all tracheids in which T_w was measured. Torus to pit aperture overlap (TPO = $(D_{tor} - D_{pa})/D_{tor}$) was calculated for all pits where both D_{tor} and at least one D_{pa} were measured. Functional tracheid lumen fraction (A_{tfx}:A_x) was calculated for each stem as many of the lignified cells within the primary xylem area were axial parenchyma and thus nonconductive; theoretical measurements based on total xylem area (A_x or A_{tx}) would overestimate actual conductivity.

Statistical methods—For each trait, assumptions of normality and residual homogeneity were analyzed, and variables were transformed if necessary. The boxcox function in the MASS package version 7.3-47

(Venables and Ripley, 2002) was used to determine transformations when the standard natural log or square root was insufficient at correcting heterogeneity of residuals. Mixed-effects models were used to account for the nonindependence of repeated measures of tracheids and pits within individual trees. All statistical analyses were performed in R Studio (RStudio Team, 2015). Model comparisons that contained at least one random factor were analyzed using likelihood ratio tests (Zuur et al., 2009; Hector, 2015). Fixed-effects models were analyzed with analysis of variance (ANOVA) type II or III to account for unbalanced measurements. Post hoc pairwise Tukey tests were performed with the lsmeans package (Lenth, 2016) for all models, which take into account random factors and ANOVA types II and III. Results were considered statistically significant at $\alpha < 0.05$.

Statistical analyses were performed on transformed variables, and therefore, all significant results are in terms of transformed scales, while some graphs and all tables of values are reported on original scales. See Appendices S2, S3, and S4 (in Supplemental Data with online version of this article) for untransformed means ± SE for areas, anatomical, and functional traits, respectively, and online Appendix S5 for all df, *t* statistics and *P* values not explicitly listed in the text. Pairwise analyses were performed on all species for all weeks, but unless otherwise noted, statistical significance is only reported for adjacent weeks. Scatter and line plots were constructed using Sigma Plot 12.5 (Systat Software, San Jose, California, USA).

RESULTS

Stem development during the first 10 wk—Images at week 2 indicated initial primary growth (i.e., elongation of the hypocotyl) comprised 2–4 discrete vascular bundles (protoxylem and early metaxylem) for *P. menziesii* and *L. occidentalis* and 4–6 clusters for *P. ponderosa*. By week 2, secondary phloem was already developing in discreet phloem bundles opposite each xylem bundle across the pith (Fig. 3A, F, K). Differentiation of primary xylem continued adjacent to the pith and then centrifugally, transitioning to secondary xylem differentiation via vascular cambium between 2 and 3 wk for *P. menziesii* and *P. ponderosa* (Fig. 4B, L). In *L. occidentalis*, differentiation and lignification of cells moved inward into the pith before secondary xylem expansion began (Fig. 4G). Within the primary xylem of all species, a substantial portion of cells appeared to be axial, lignified parenchyma. Much like the pits between adjacent tracheids and rays (Esau, 1977), the tracheid to axial parenchyma pits were also half-bordered pits, with a bordered pit on the tracheid side and a simple pit on the parenchyma side; half-bordered pits were present in both lignified and nonlignified parenchyma adjacent to tracheids near the pith. In some cases, the middle lamella did not appear to thicken into a torus-like structure (online Appendix S6).

A Casparian strip or suberized endodermis was present in all species from week 2 (best visualized in *P. ponderosa*; Fig. 4K–O) and by week 6 for all species, the vascular bundle along with the endodermis had expanded enough to collapse and compact the ground tissue against the initial stem epidermis. Also by this time, the phellogen (i.e., cork cambium) was well visualized in all species (Fig. 4D, I, N). Between weeks 6 and 10, the periderm further developed and expanded; by week 10, all three components of the periderm (phellem, phellogen, and phelloderm) (Esau, 1977) were present in all three species. By this age, the periderm had expanded enough to induce splitting and shedding of the original epidermal layer in all three species (Fig. 4E, J, O), effectively beginning replacement of the initial epidermal layer with the periderm (Esau, 1977). *Larix occidentalis* and *P. menziesii* only had statistically significant increases in A_s between weeks 6 and 10 (Appendix S5), while statistical significance could not be evaluated for *P. ponderosa* (due to a $n = 1$ stem diameter measurement for week 10 as these stems were larger than our smallest available objective lens).

Within the primary epidermis of stems of *P. ponderosa*, frequent, sunken stomata and associated guard and subsidiary cells were observed (Appendix S7). Structure of the stomata appeared similar to those reported in *Pinus* leaves (Esau, 1977). No stomata were observed in the developing periderm. These stomata were not observed in the other two species at any age, but they have also been observed in very young stems of *Pinus monticola* (M. L. Miller, unpublished data).

Four to six initial primary resin ducts were visible in *P. ponderosa* by the second week (Fig. 4K), and some irregularly spaced ducts were observed in *L. occidentalis* by week 10 (Fig. 4J), but no resin ducts were visible in *P. menziesii* at any time period.

Xylem anatomical and plant functional traits—*Xylem characteristics—Larix occidentalis* and *P. ponderosa* showed significant increases in xylem cross-sectional area (A_x), from weeks 3 to 4 and weeks 6 to 10, while A_x in *P. menziesii* significantly increased between weeks 4 to 6 and 6 to 10 (Appendix S5). For all time periods, A_x differed significantly among all three species where *L. occidentalis* had the smallest A_x and *P. ponderosa* had the largest, with the exception of week 10, when the A_x of *L. occidentalis* exceeded that of *P. menziesii*. In contrast, *L. occidentalis* and *P. menziesii* had similar total functional xylem areas (A_{tfx}) for weeks 2 through 6, while *P. ponderosa* was significantly higher for all time periods (Fig. 5B, solid lines). A_{tfx} increased significantly in all species between all weeks except for weeks 4 to 6 for *P. ponderosa* and weeks 3 to 4 for *P. menziesii*. At week 10, differences between species were significant with *P. ponderosa*, *L. occidentalis*, and *P. menziesii* representing descending order of total functional xylem area.

Histograms of lumen diameters for all species displayed right-skewed distributions with shifting means per time period per species (Fig. 6A–C). Tracheid lumen for *P. menziesii* decreased significantly in diameter between weeks 4 to 6 and between several nonadjacent weeks including weeks 2 to 6 and 4 to 10, illustrating a decrease over time, while the differences for *L. occidentalis* were not significantly different among any weeks. D_t for *P. ponderosa* significantly increased between weeks 2 and 3 and subsequently decreased between week 3 to 6 and week 4 to 10. Initially, there were no significant differences in mean D_t between species, but by week 10, *P. menziesii* had significantly smaller mean tracheid lumen compared with the other two species, which did not differ significantly from each other. However, between weeks 2 and 10, *P. ponderosa* had the largest lumen diameters compared with the other two species. Overall, lumen distributions illustrated that *P. ponderosa* had the widest distribution of the largest tracheids, especially during intermediate growth, while *P. menziesii* exhibited the narrowest distribution range combined with the smallest lumen diameters at the latter time periods.

When averaged across all species, mean D_t significantly increased between weeks 2 to 3 and decreased between weeks 4 to 6, while cell wall thickness significantly increased between each time period.

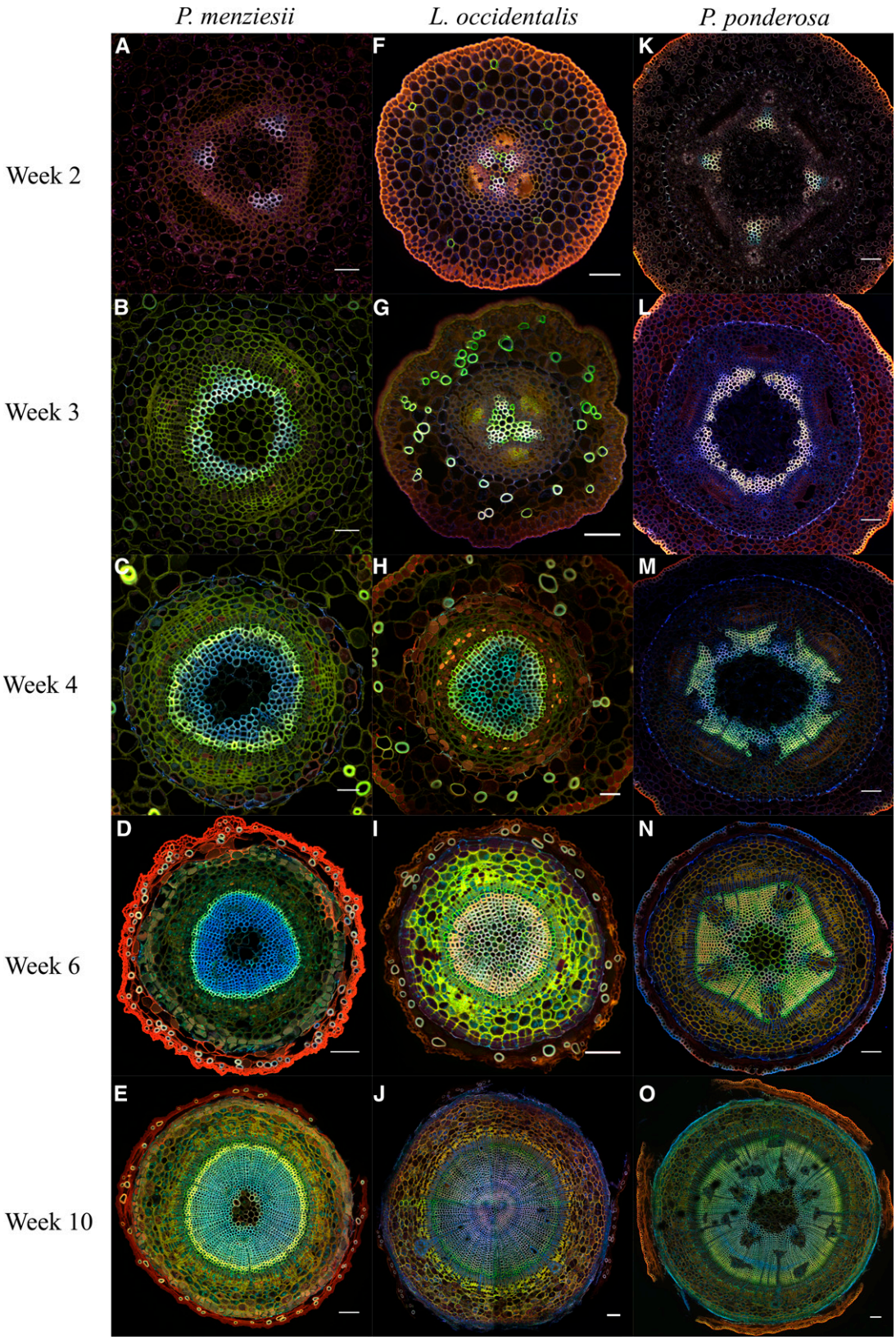

FIGURE 4 Vascular development over 10 wk. Xylem development in (A–E) *Pseudotsuga menziesii*, (F–J) *Larix occidentalis*, and (K–O) *Pinus ponderosa* imaged with confocal laser scanning microscopy (CLSM) at 2 (A, F, K), 3 (B, G, L), 4 (C, H, M), 6 (D, I, N) and 10 (E, J, O) weeks after planting. Differences in coloration are attributed to differing stain concentrations, system settings, and image processing. Bars = 100 µm. CLSM system settings and image postprocessing parameters for each image are available in Appendix S1.

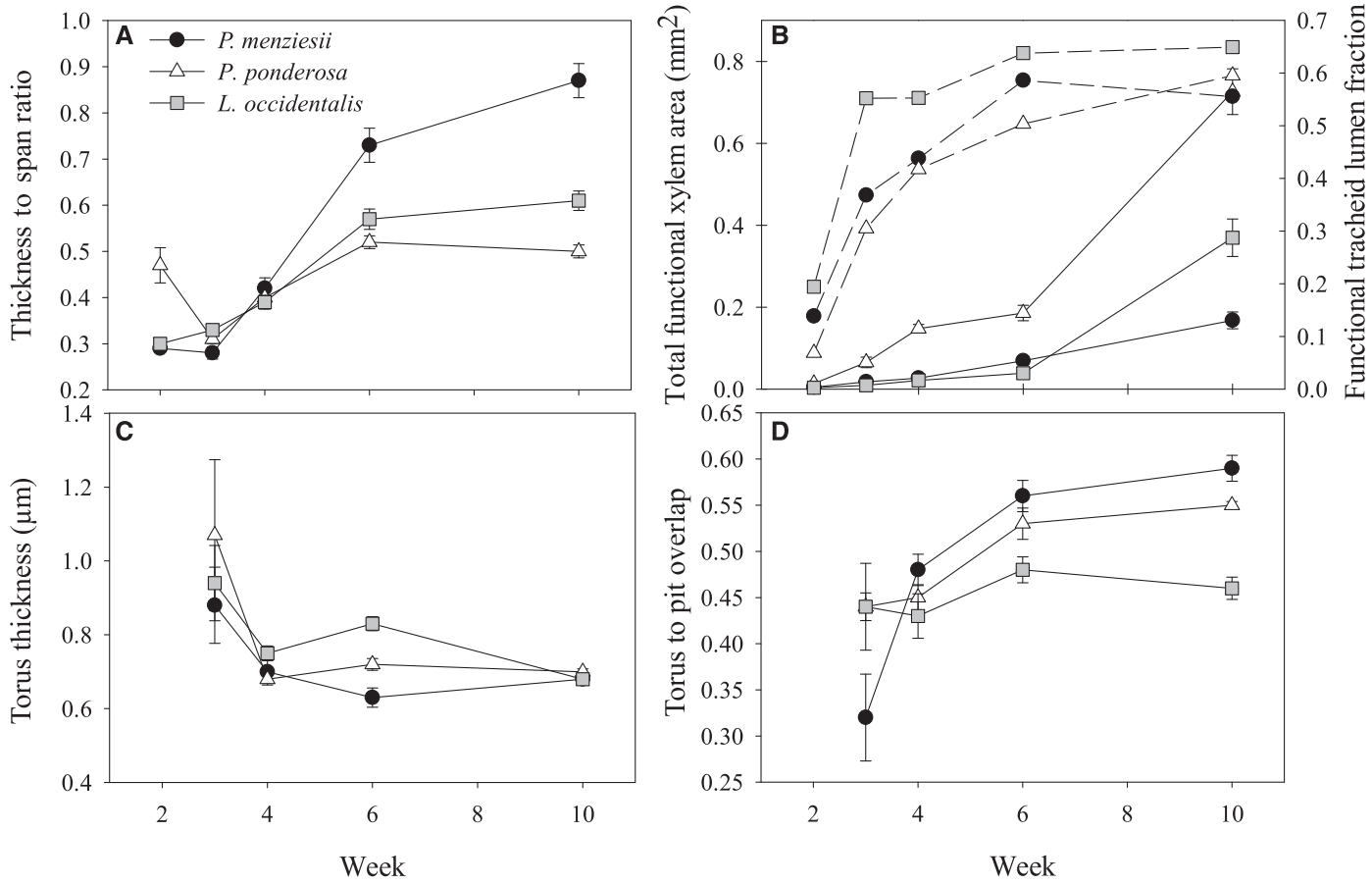

FIGURE 5 Xylem anatomical and functional characteristics. (A) Thickness to span ratio (T_w/D_t) is the ratio of tracheid cell wall thickness to the diameter of the tracheid, (B) total functional xylem area (A_{tfx}; solid lines) and functional tracheid lumen fraction (A_{tfx}:A_x; dashed lines), (C) estimated torus thickness (T_t), and (D) torus to pit aperture overlap (TPO). Week 2 results not included in panels C and D due to very low torus sample sizes. Error bars are standard errors.

D_t and T_w were nearly independent of one another, but did exhibit a very slight statistically significant negative correlation (slope: −0.01, adjusted $R^2 = 0.004$, $P = 0.002$). Averaged over all species, T_w/D_t increased from week to week with significant increases between weeks 3 to 4 and 4 to 6, indicating that tracheid wall thickness, as opposed to tracheid diameter, governed changing T_w/D_t ratios in growing seedlings. Initially, *P. ponderosa* had the largest T_w/D_t, but by week 6, *P. menziesii* had significantly greater T_w/D_t compared with the other two species (Fig. 5A). When only weeks 2 and 10 are compared, *L. occidentalis* and *P. menziesii* both had overall significant increases in T_w/D_t, while *P. ponderosa* seedlings had no significant change.

The functional tracheid lumen fraction (A_{tfx}:A_x) tended to increase over time, but eventually stabilized as there were no significant changes between weeks 6 and 10 for any species (Fig. 5B, dotted lines). Although *L. occidentalis* had the lowest absolute value of total functional xylem area for 4 of the 5 time periods, it had the greatest tracheid lumen fraction when averaged over all weeks, while *P. ponderosa* had the lowest fraction.

Pit characteristics—There were positive correlations between membrane diameter (D_m) and torus diameter (D_{tor}) ($R^2 = 0.59$; $P < 0.0001$) and between D_m and pit aperture (D_{pa}) ($R^2 = 0.44$, $P < 0.0001$) as well as D_{tor} to D_{pa} ($R^2 = 0.32$, $P < 0.0001$). Torus thickness (T_t) was not correlated with any other pit feature with the exception of a slight positive correlation with D_{tor} ($R2 = 0.009$; $P = 0.03$). Tori within the primary xylem were significantly thicker across all species compared to tori within the secondary xylem, though intraspecific analyses showed that differences between primary and secondary xylem T_t were not significant in *P. menziesii*. Averaged across species, T_t decreased over the first three time periods, indicating a transition in the dominant xylem type from primary to secondary xylem within all seedlings (Fig. 5C; Appendix S3). Averaged across xylem type and time periods, *L. occidentalis* had the largest T_t compared with the other two species, which were not significantly different from one another.

Primary xylem had smaller TPOs compared with secondary xylem averaged over all weeks and species; in some cases, primary xylem TPOs were negative (not shown), indicating that the torus diameter was smaller than the pit aperture. In terms of secondary xylem, *L. occidentalis* had the smallest overlap when averaged over all time periods, while *P. ponderosa* and *P. menziesii* were not significantly different from one another. However, by week 10, secondary xylem in *P. menziesii* had a significantly larger TPO compared with the other two species, while *L. occidentalis* remained the smallest (Fig. 5D).

Additional functional traits—Theoretical stem conductance $K_{h(t)}$ per week, averaged across all species, significantly increased over time, and by week 10, all species differed significantly from one

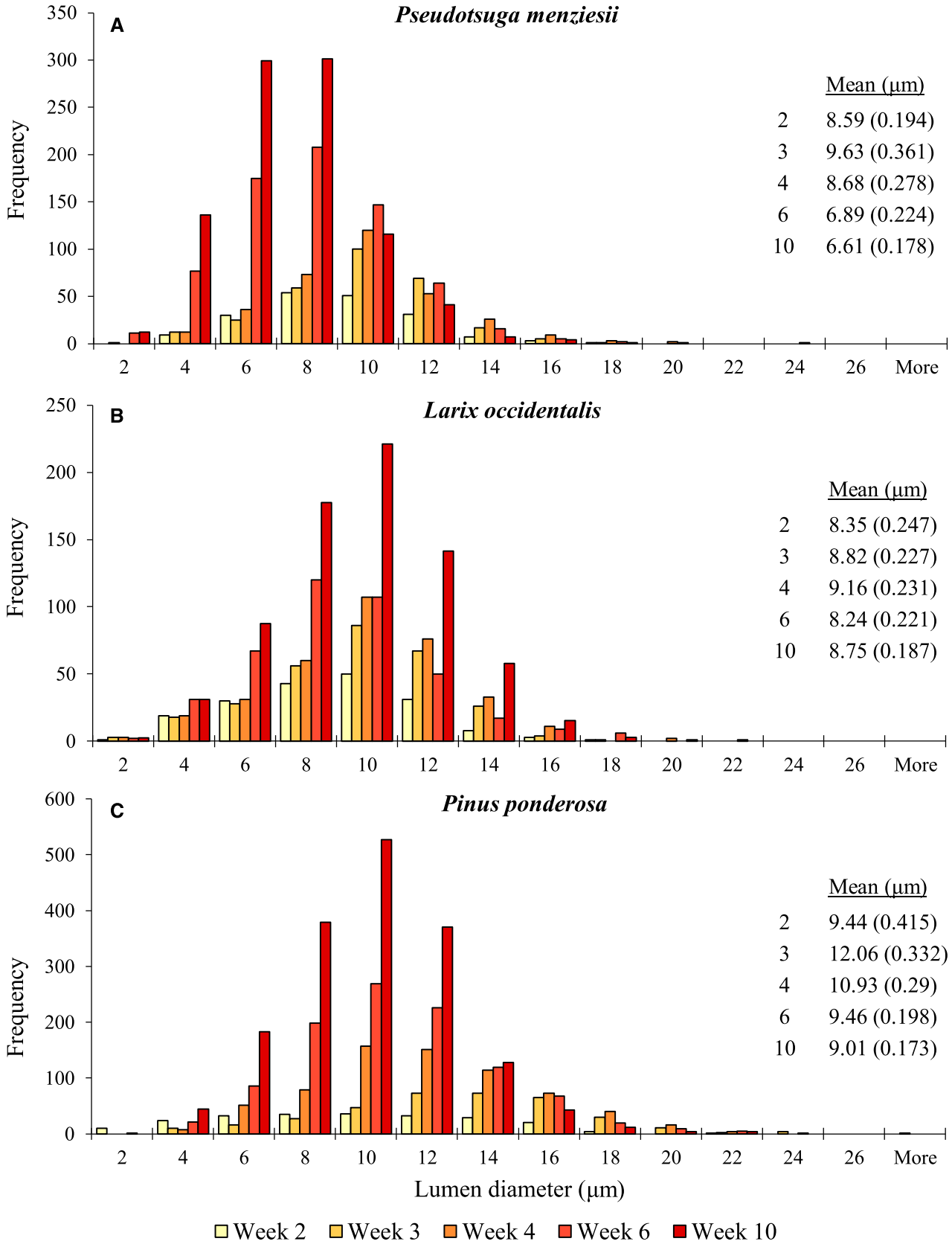

FIGURE 6 Tracheid lumen diameter distributions for (A) *Pseudotsuga menziesii*, (B) *Larix occidentalis*, and (C) *Pinus ponderosa*. Means provided are mean lumen diameters per week with (SE). *P. ponderosa* and *L. occidentalis* frequencies were adjusted by 0.5 for weeks 6 and 10 due to higher numbers of tracheids measured as compared with the other weeks.

another with *P. ponderosa* having the greatest conductance and *P. menziesii* the lowest (not shown). When normalized by functional xylem area (i.e., theoretical xylem specific conductivity $K_{s(t)}$), conductivity significantly decreased between weeks 4 to 6 and 6 to 10. When normalized by leaf area (i.e., theoretical leaf specific conductivity $K_{L(t)}$), conductivity increased from weeks 2 to 6 followed by a statistically significant decrease from weeks 6 to 10, although increases between adjacent weeks from 2 to 6 were not significant, the difference between weeks 2 and 6 was significant.

Intraspecific analyses over time demonstrated different trends in $K_{s(t)}$ and $K_{L(t)}$ per species (Fig. 7A, B). $K_{s(t)}$ appeared to decrease through time for all species, although changes among time periods for *L. occidentalis* were not significantly different (Fig. 7A). Differences were not statistically significant between adjacent time periods for *P. ponderosa*, but there were significant decreases between weeks 3 to 6 and weeks 4 to 10. $K_{s(t)}$ for *P. menziesii* significantly decreased between weeks 4 to 6 and weeks 6 to 10. $K_{L(t)}$ dropped significantly for all species between weeks 6 and 10. Conversely, leaf area for all species expanded rapidly between weeks 6 and 10, similar to the increase in functional xylem area; *P. ponderosa* had the greatest leaf area development (Fig. 7C). The decrease in $K_{L(t)}$ with an increasing leaf area indicates that crown expansion exceeded the xylem area expansion for the same time period; thus, changes in leaf area as opposed to changes in xylem area governed changes in $K_{L(t)}$. Although $K_{L(t)}$ fluctuated over time, there were ultimately no statistically significant differences for any species between the first and last time periods. The drop in $K_{L(t)}$ at week 2 for *L. occidentalis* was likely biased lower by $n = 2$ crown measurements for this time period (both individuals had larger than average leaf areas).

Leaf area to sapwood area (A_L:A_s) is a frequently reported trait that has numerous implications for dry climate adaptation (e.g., Tyree and Zimmermann, 2002; Maherali et al., 2002). In our case, we used A_{tfx} as our sapwood analog because it is the portion of the xylem assumed to be functional in transporting water to the crown. When averaged across species, A_L:A_{tfx} decreased between all time periods from week 3 to week 6 in all species and then increased between week 6 and 10. However, a breakdown within species showed that this trend held true only for *L. occidentalis*. There were no significant differences between any adjacent time periods for *P. ponderosa*, although the decrease between week 2 to 6 was significant ($P = 0.0001$). *Pseudotsuga menziesii* also had a significant decrease between week 2 to 6 followed by a significant increase between weeks 6 and 10. At week 2, *L. occidentalis* had the smallest A_L:A_{tfx} as compared with the other two species, but by week 10, *L. occidentalis* was significantly larger that *P. menziesii* and not significantly different from *P. ponderosa*. An alternate way of analyzing the change in A_L to A_{tfx} over time was to examine A_L as a function of A_{tfx} (Fig. 8), where the slope of the line between any two adjacent time points represents the ratio of crown to xylem area (i.e., A_L:A_s). The steepest slope occurred from weeks 6 to 10 for *P. menziesii*, which is consistent with *P. menziesii* exhibiting the largest A_L:A_{tfx} by week 10.

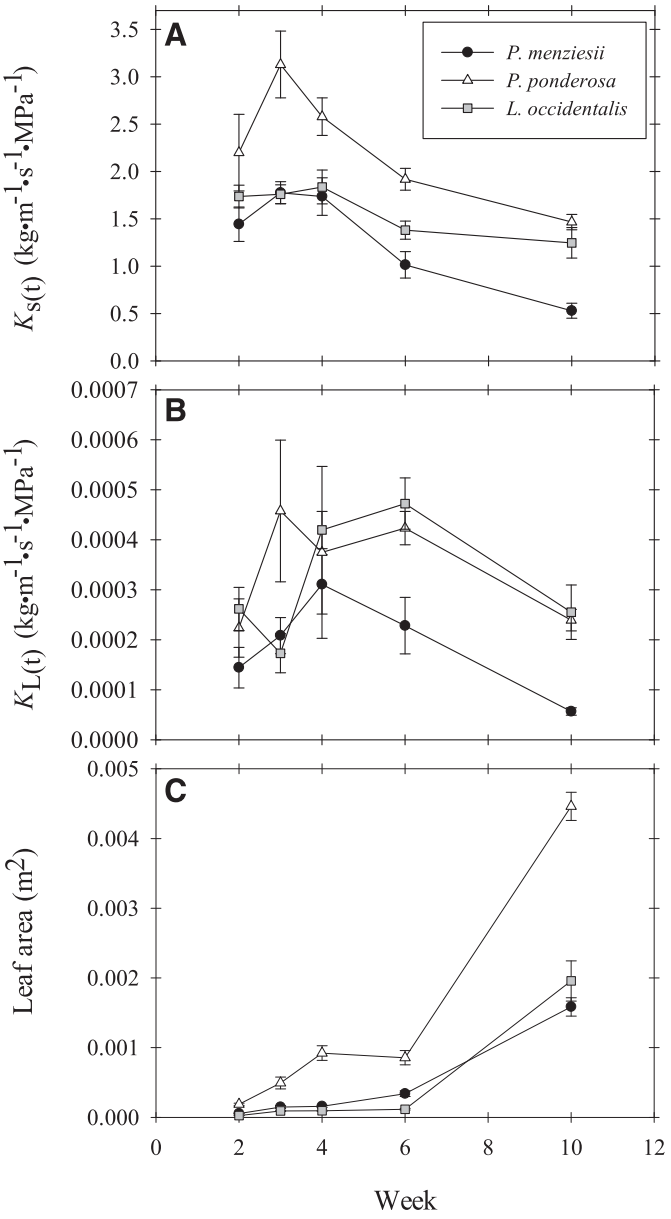

FIGURE 7 $K_{s(t)}$, $K_{L(t)}$, and A_L over time for all species. (A) Theoretical xylem specific conductivity $K_{s(t)}$, (B) theoretical leaf specific conductivity $K_{L(t)}$, and (C) absolute crown leaf area A_L averaged per species per time period with error bars (SE).

DISCUSSION

Anatomical and functional traits during the first 3 wk—Theoretical hydraulic conductivity of seedlings within the first 2 to 3 wk was higher than in their older counterparts on a per functional xylem area basis due to their larger tracheid lumens, which enable greater water transport to the crown per xylem area (Tyree and Zimmermann, 2002; Sperry et al., 2006). However, actual conductivity depends on additional factors, and estimates of maximum hydraulic capabilities overestimate in vitro hydraulic measurements of conductivity (Tyree and Ewers, 1991; Tyree and Zimmermann, 2002; Santiago et al., 2004; Nolf et al., 2017). Evidence in a growing body of recent literature supports the hypothesis that xylem conductivity in conifers is inherently dependent upon pits in general, where the wider pits (D_m) and more frequent and larger margo pores allow for greater water transport capacity to a point (see Schulte et al., 2015 and references therein; but see Hacke et al., 2004).

Even though the very young germinants exhibited higher theoretical conductivities, they appeared to be less able to mitigate hydraulic dysfunction with smaller T_w/D_t and TPO values, which are

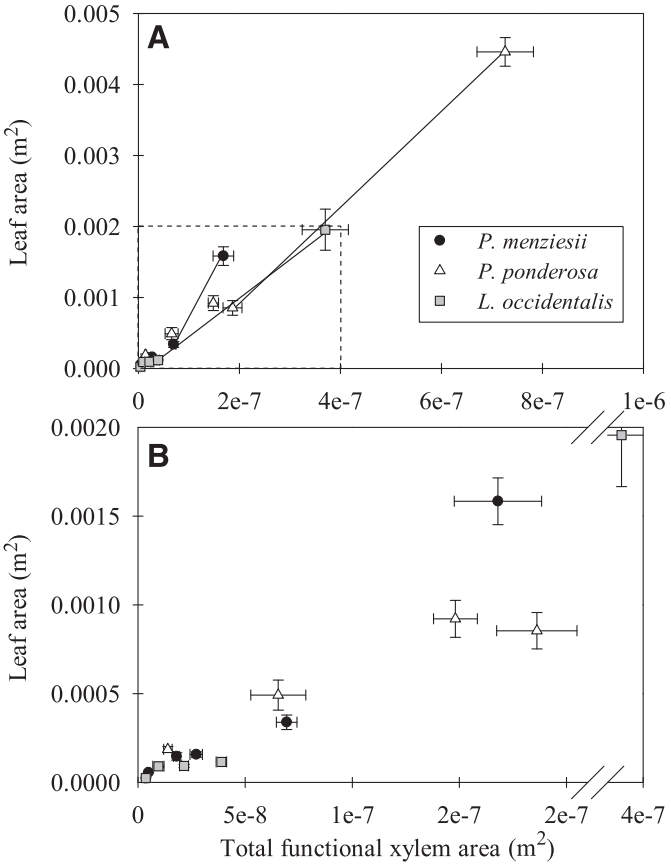

FIGURE 8 Leaf area to total functional xylem area. (A) Each point represents the mean of each species per respective time period (2, 3, 4, 6, and 10 wk). The slope of the line between adjacent points is the leaf area to sapwood area ratio. (B) Enlargement of area delineated in panel A. Close proximity to the origin and short spacing of the first four points for *Pseudotsuga menziesii* and *Larix occidentalis* (lower left corner) indicate minimal functional xylem and leaf area expansion during the first 3 to 4 time periods. Error bars are standard errors.

less resistant to tracheid implosion (Sperry et al., 2006) and air seeding (expansion of air from one tracheid into an adjacent water-filled tracheid), respectively (Hacke et al., 2004; Delzon et al., 2010; Jansen et al., 2012; Bouche et al., 2014). While tracheid implosion is not frequently observed in situ (with implosion pressures being generally more negative than embolism pressure) (Hacke et al., 2004, 2006; Sperry et al., 2006; Domec et al., 2009), implosion may occur within the protoxylem, in which the cell walls are only helically thickened (Appendix S8) and have been shown to mechanically deform during stem growth (Esau, 1977).

A large TPO generally confers a better ability to seal off embolized tracheids (Delzon et al., 2010; Bouche et al., 2014). Across all species, primary xylem had smaller TPOs in general and, in some cases, (especially in *L. occidentalis*) negative values, indicating that the torus diameter was smaller than the pit aperture, which would likely be ineffective in preventing air seeding. However, visualization of tori at week 2 were surprisingly infrequent even though large pits were regularly observed. Primary xylem also exhibited smaller T_w/D_t values overall, although T_w/D_t has been shown to negatively correlate with P_{50} regardless of actual observed implosion (Sperry et al., 2006). Our findings that T_w governed changes in T_w/D_t corroborate findings by Bouche et al. (2014), while others have found that T_w remained relatively constant, and thus, D_t governed changes in T_w/D_t (Pittermann et al., 2006a; Sperry et al., 2006).

All species were producing secondary xylem via a vascular cambium by week 3, although *L. occidentalis* was the only species with lignified xylem and axial parenchyma within the entirety of the pith area. Axial, lignified parenchyma no doubt contributes to mechanical stability at younger stages by reducing the potential for Brazier buckling (Spatz and Niklas, 2013), but the presence of lignin may also indicates that the axial parenchyma are, to some extent, under tension.

The discovery of stomatal apparatus within the stem primary epidermis of *P. ponderosa* was surprising, as stomata in stems are common in some angiosperm families (especially Fabaceae) (Pfanz et al., 2002), but are rare in extant gymnosperms (i.e., *Ephedra*) (Romberger et al., 2004; Ávila et al., 2014). To our knowledge, the presence of stem stomata has not been reported in any extant conifer seedlings. While stem photosynthesis without the presence of stomata is common (Pfanz et al., 2002; Pallardy, 2008), it is often associated with refixation of respired CO_2, whereas stem photosynthesis with concurrent stomata are associated with fixation of atmospheric CO_2 (see review by Ávila et al., 2014). Stomata in the epidermis may confer an added benefit for *P. ponderosa* seedlings, allowing for potential large photosynthetic fluxes given adequate conditions during very early growth. Enhanced photosynthetic capacity, in turn, may facilitate extended root and canopy growth, giving the seedlings a competitive advantage at a very early age. Active gas exchange within the stem may also facilitate quicker osmotic adjustments to ease xylem tension as well as provide additional stem cooling while transpiring (Lambers et al., 2008). Further research will be necessary to determine the actual contribution of stem photosynthesis to plant net CO_2 fixation.

Anatomical and functional traits by week 10—Between weeks 3 and 10, the seedlings underwent substantive xylem expansion and anatomical development. Functional characteristics at week 10 effectively represented traits reflective of secondary xylem with smaller tracheid diameters, thicker cell walls, thinner tori, and larger torus to aperture overlaps. Surprisingly, for many of the functional traits including $K_{s(t)}$, $K_{L(t)}$, and T_w/D_t, *L. occidentalis* and *P. ponderosa* were not significantly different by week 10, although *P. ponderosa* had the highest A_L, A_{tfx}, and $K_{h(t)}$. The largest A_L, A_{tfx}, and $K_{h(t)}$ in *P. ponderosa* seedlings are likely indicative that *P. ponderosa* can transport larger quantities of water, which increases the potential for photosynthesis and growth compared with the other seedlings at this age (Santiago et al., 2004; Brodribb et al., 2005). Indeed, we observed that *P. ponderosa* crown and xylem growth increased across all time periods and at a higher rate than the other species, which likely necessitated greater mechanical stability.

By week 10, *P. menziesii* seedlings exhibited the largest A_L:A_{tfx}, TPO, and T_w/D_t, while simultaneously exhibiting the lowest $K_{h(t)}$, A_{tfx}, $K_{s(t)}$, $K_{L(t)}$. The seedling-specific characteristics of *P. menziesii* at week 10 present a strong argument for the safety vs. efficiency trade-off (Zimmermann, 1983; Pittermann et al., 2006b; but see Gleason et al., 2016), in which the xylem of *P. menziesii* is likely more resistant to embolism, air seeding, and tension-induced implosion, but at the cost of hydraulic efficiency. The larger A_L:A_{tfx} indicates that a smaller xylem area supplies a given crown area, implying that *P. menziesii* would have a more negative water potential

for a given transpiration rate and that dysfunction within a given xylem area may have a greater impact on crown water availability compared with the other two species (Lambers et al., 2008); thus the larger A_L:A_{tfx} would necessitate more embolism-resistant xylem in order to be competitive with the other two species, which is what the anatomy of these seedlings suggests. However, comparisons based strictly on A_L:A_{tfx} do not take into account other physiological and morphological characteristics such as water-use efficiency, degree of isohydry, and rooting depth, which may make *P. ponderosa* more competitive in xeric conditions.

Larix occidentalis had the lowest A_L:A_{tfx} ratio and the highest tracheid lumen fraction but the lowest torus to pit aperture overlap and largest torus thickness. The low TPO (Appendix S4) is most likely indicative of *L. occidentalis* being the least resistant to hydraulic dysfunction via air seeding. However, the high tracheid lumen fraction of *L. occidentalis* illustrated that, in terms of carbon investment strategies, *L. occidentalis* may be more efficient in carbon allocation for xylem construction, whereby a greater proportion of xylem built is functional in water transport in the young seedlings. As illustrated in Figs. 5 and 7 (dotted lines), *L. occidentalis* did not require the additional mechanical support of secondary xylem until after week 6, when the seedlings experienced substantial stem, xylem, and crown growth.

Contrary to our hypothesis, by week 10, xylem of *P. menziesii* appeared to be the most embolism resistant, followed by *P. ponderosa* and then *L. occidentalis*, based on torus to pit aperture overlap, thickness to span ratio, and torus thickness as implied by the correlations of these traits to P_{50} values in previous studies (Hacke et al., 2001; Hacke and Sperry, 2001; Pittermann et al., 2006b; Domec et al., 2009; Delzon et al., 2010; Sterck et al., 2012; Bouche et al., 2014; Schulte et al., 2015). Corroborating our findings, and despite relative drought tolerances and historical ranges of the species, research on saplings and mature trees have found that *P. menziesii* has more embolism-resistant roots, shoots, and branches than *P. ponderosa* does (Piñol and Sala, 2000; Stout and Sala, 2003; see also reviews by Martínez-Vilalta et al., 2004 and Barnard et al., 2011). Little research has included hydraulic measurements of *L. occidentalis*; however, Piñol and Sala (2000) found no statistical difference in branch P_{50} between *L. occidentalis* and *P. menziesii*.

Correlations among A_s, A_{tx}, and A_{tfx}—Stem diameter is often used as a proxy for functional sapwood area in adult trees and is the basis for many allometric scaling relationships (Vertessy et al., 1995; Bond-Lamberty et al., 2002). In the current study, correlations between the different area measurements were analyzed to see whether an easily measured variable, such as stem area, could be used as a predictor for functional xylem area, which is much more time-consuming to calculate. The correlation between A_s and A_{tfx} was relatively poor, indicating that predictions of functional xylem area cannot be accurately predicted as a function of stem cross-sectional area (R^2 = 0.38, and $P < 0.0001$) during early seedling development. Interestingly, there was a very strong correlation between measured A_{tx} and estimated A_{tfx} averaged across all species and all time periods (R^2 = 0.98, $P < 0.0001$). However, it was not a 1:1 relationship (i.e., slope), which indicates that extrapolating actual total functional xylem is necessary for young seedlings. However, once the relationship is known, A_{tfx} could be accurately predicted from A_{tx} for all three species across all time periods, where A_{tx} is a relatively simple and rapid measurement as compared with A_{tfx}.

Air seeding and torus thickness—In conifers, there are several hypotheses in regards to pit air seeding mechanisms: torus displacement (Hacke et al., 2004; Domec et al., 2006), seal capillary seeding (Delzon et al., 2010), torus capillary seeding (Jansen et al., 2012; Bouche et al., 2014), and potentially torus prolapse (Zelinka et al., 2015). With a smaller TPO, the membrane is not as effective sealing off the embolized conduit, which would facilitate seal capillary seeding or torus displacement. Several studies have concluded that, due to the correlation between TPO and cavitation, the most likely mechanisms for air seeding occur at the torus–pit aperture interface (Delzon et al., 2010; Pittermann et al., 2010; Bouche et al., 2014), though there is some additional support for torus pore air seeding in Pinaceae (Jansen et al., 2012; Bouche et al., 2014).

However, torus thickness remains an understudied but potentially critical anatomical component (Schulte et al., 2015). Mechanical-displacement experiments by Zelinka et al. (2015) showed the torus itself to be surprisingly flexible. We hypothesize here that thicker tori may be less flexible and reduce sealing capacity when aspirated and thus would be more prone to seal capillary seeding, which would be further exacerbated by a small TPO. However, a thicker torus may reduce torus capillary seeding and the potential for torus prolapse. Incorporating T_w/D_t, TPO, and T_t results, we expect that protoxylem, metaxylem, then secondary xylem would be the order of increasing resistance to embolism and air seeding.

To our surprise, our results indicate that torus thickness is either not correlated or only very slightly correlated with any other pit anatomical or functional characteristic, including TPO (P = 0.08). Its independence from other traits indicates that it may be a coevolved feature that inherently plays a causative role in embolism resistance, though teasing apart the influences between TPO and T_t will be necessary in future research.

Lumen diameter distributions—*Pinus ponderosa* distributions were skewed farther right than the other two species, meaning it had greater numbers of very large tracheids. Larger tracheids imply not only a greater capacity to transport water, but also the potential to maintain hydraulic function during desiccation. For example, even if the largest conduits embolized during dehydration, *P. ponderosa* seedlings would still be capable of transporting a significant amount of water. Additionally, *P. ponderosa*, which had the smallest functional tracheid lumen fraction and conversely may have the greatest parenchyma area, which may give *P. ponderosa* seedlings a competitive advantage in xeric conditions by facilitating necessarily rapid adjustments in osmotica or via xylem refilling (Johnson et al., 2011; McCulloh et al., 2011).

CONCLUSIONS

Considerable changes in anatomy over the initial 10-wk growth period are indicative of potentially drastic changes in embolism resistance depending on the developmental stage and the species. Therefore, seedling age at the onset of in situ limited water availability is likely to impact species-specific survivability, especially considering lack of additional mitigating factors, such as deep roots and capacitive stores. Differing impacts of water limitations across species may in turn alter species distributions and local species abundance, especially in localities where these species cohabitate.

With such substantial differences in key morphological and functional traits, we would also expect subsequent in vitro vulnerability

curves generated during early seedling development to be species-age specific. Our results, combined with the sparse research available on first year species-specific seedlings (Cui and Smith, 1991; Urli et al., 2013; M. L. Miller, unpublished data) and available data from mature specimens, indicate that parameters and relationships derived from adult counterparts cannot be extrapolated to the early seedling stage.

This research has elucidated species-specific xylem development and functional properties, which in turn inform upon changing potential maximum hydraulic capabilities, carbon investment priorities, water transport strategies, and resistance to drought-induced hydraulic dysfunction as these seedlings transition from primary to secondary growth. One particular aspect of conifer seedling development that should be included in future work would be SEM or TEM analyses of tracheid torus-margo structures. Little is known about these pit characteristics in young seedlings, particularly in the primary xylem of a newly germinated seedling, and torus-margo structure may be closely related to drought-tolerance in early growth stages.

ACKNOWLEDGEMENTS

Research reported in this publication was supported by the National Science Foundation grant #IOS-1146746, University of Idaho C. R. Stillinger Forest Science Research Fellowship, and an Institutional Development Award (IDeA) from the National Institute of General Medical Sciences of the National Institutes of Health under grant # P30 GM103324. The authors thank Ann Norton (Director of the IBEST Imaging Core at the University of Idaho), Jason Schlafmann, Kathryn Baker, Forrest Sherman, Eric Larson, Molly Rard, Ryan Spaniel, Laura Young, Laurie Bell, and Dario Paiva. The authors also thank Katherine McCulloh and three anonymous reviewers for providing valuable feedback, which resulted in a significantly improved manuscript.

LITERATURE CITED

Anderegg, W. R. L., and L. D. L. Anderegg. 2013. Hydraulic and carbohydrate changes in experimental drought-induced mortality of saplings in two conifer species. *Tree Physiology* 33: 252–260.

Ávila, E., A. Herrera, and W. Tezara. 2014. Contribution of stem CO_2 fixation to whole-plant carbon balance in nonsucculent species. *Photosynthetica* 52: 3–15.

Barnard, D. M., F. C. Meinzer, B. Lachenbruch, K. A. McCulloh, D. M. Johnson, and D. R. Woodruff. 2011. Climate-related trends in sapwood biophysical properties in two conifers: Avoidance of hydraulic dysfunction through coordinated adjustments in xylem efficiency, safety and capacitance. *Plant, Cell & Environment* 34: 643–654.

Bond, J., L. Donaldson, and K. Hitchcock. 2008. Safranin fluorescent staining of wood cell walls. *Biotechnic & Histochemistry* 83: 161–171.

Bond-Lamberty, B., C. Wang, and S. T. Gower. 2002. Aboveground and belowground biomass and sapwood area allometric equations for six boreal tree species of northern Manitoba. *Canadian Journal of Forest Research* 32: 1441–1450.

Bouche, P. S., M. Larter, J.-C. Domec, R. Burlett, P. Gasson, S. Jansen, and S. Delzon. 2014. A broad survey of hydraulic and mechanical safety in the xylem of conifers. *Journal of Experimental Botany* 65: 4419–4431.

Brodribb, T. J., N. M. Holbrook, M. A. Zwieniecki, and B. Palma. 2005. Leaf hydraulic capacity in ferns, conifers and angiosperms: Impacts on photosynthetic maxima. *New Phytologist* 165: 839–846.

Burns, R. M., and B. H. Honkala [tech. coords.]. 1990. Silvics of North America: 1. Conifers; 2. Hardwoods. USDA Forest Service Agriculture Handbook 654, Washington, D.C., USA.

Clark, J. S., L. Iverson, C. W. Woodall, C. D. Allen, D. M. Bell, D. C. Bragg, A. W. D'Amato, et al. 2016. The impacts of increasing drought on forest dynamics, structure and biodiversity in the United States. *Global Change Biology* 22: 2329–2352.

Corcuera, L., E. Gil-Pelegrin, and E. Notivol. 2012. Differences in hydraulic architecture between mesic and xeric *Pinus pinaster* populations at the seedling stage. *Tree Physiology* 32: 1442–1457.

Cui, M., and W. K. Smith. 1991. Photosynthesis, water relations and mortality in *Abies lasiocarpa* seedlings during natural establishment. *Tree Physiology* 8: 37–46.

Delzon, S., C. Douthe, A. Sala, and H. Cochard. 2010. Mechanism of water-stress induced cavitation in conifers: Bordered pit structure and function support the hypothesis of seal capillary-seeding. *Plant, Cell & Environment* 33: 2101–2111.

Domec, J.-C., B. Lachenbruch, and F. Meinzer. 2006. Bordered pit structure and function determine spatial patterns of air-seeding thresholds in xylem of Douglas-fir (*Pseudotsuga menziesii*; Pinaceae) trees. *American Journal of Botany* 93: 1588–1600.

Domec, J.-C., J. M. Warren, F. C. Meinzer, and B. Lachenbruch. 2009. Safety factors for xylem failure by implosion and air-seeding within roots, trunks and branches of young and old conifer trees. *International Association of Wood Anatomists Journal* 30: 100–120.

Esau, K. 1977. Anatomy of seed plants, 2nd ed. John Wiley, Toronto, Ontartion, Canada.

Facelli, J. M. 2008. Specialized strategies I: Seedlings in stressful environments? *In* M. A. Leck, V. T. Parker, and R. L. Simpson [eds.], Seedling ecology and evolution, 57–78. Cambridge University Press, Cambridge, UK.

Gleason, S. M., M. Westoby, S. Jansen, B. Choat, U. G. Hacke, R. B. Pratt, R. Bhaskar, et al. 2016. Weak tradeoff between xylem safety and xylem-specific hydraulic efficiency across the world's woody plant species. *New Phytologist* 209: 123–136.

Hacke, U. G., and J. S. Sperry. 2001. Functional and ecological xylem anatomy. *Perspectives in Plant Ecology, Evolution and Systematics* 4: 97–115.

Hacke, U. G., J. S. Sperry, and J. Pittermann. 2004. Analysis of circular bordered pit function II. Gymnosperm tracheids with torus-margo pit membranes. *American Journal of Botany* 91: 386–400.

Hacke, U. G., J. S. Sperry, W. T. Pockman, S. D. Davis, and K. A. McCulloh. 2001. Trends in wood density and structure are linked to prevention of xylem implosion by negative pressure. *Oecologia* 126: 457–461.

Hacke, U. G., J. S. Sperry, J. K. Wheeler, and L. Castro. 2006. Scaling of angiosperm xylem structure with safety and efficiency. *Tree Physiology* 26: 689–701.

Hector, A. R. 2015. The new statistics with R: An introduction for biologists. Oxford University Press, New York, New York, USA.

Hepler, P. K., and B. E. S. Gunning. 1998. Confocal fluorescence microscopy of plant cells. *Protoplasm* 201: 121–157.

Horton, T. R., and M. G. A. van der Heijden. 2008. The role of symbioses in seedling establishment and survival. *In* M. A. Leck, V. T. Parker, and R. L. Simpson [eds.], Seedling ecology and evolution, 189–213. Cambridge University Press, Cambridge, UK.

Jansen, S., J. B. Lamy, R. Burlett, H. Cochard, P. Gasson, and S. Delzon. 2012. Plasmodesmatal pores in the torus of bordered pit membranes affect cavitation resistance of conifer xylem. *Plant, Cell & Environment* 35: 1109–1120.

Jansen, S., A. Pletsers, and Y. Sano. 2008. The effect of preparation techniques on SEM-imaging of pit membranes. *International Association of Wood Anatomists Journal* 29: 161–178.

Johnson, D. M., K. A. McCulloh, and K. Reinhardt. 2011. The earliest stages of tree growth: Development, physiology and impacts of microclimate. *In* F. C. Meinzer, B. Lackenbruch, and T. E. Dawson [eds.], Size- and age-related changes in tree structure and function, 65–87. Springer, Dordrecht, Netherlands.

Kerr, K. L., F. C. Meinzer, K. A. McCulloh, D. R. Woodruff, and D. E. Marias. 2015. Expression of functional traits during seedling establishment in two populations of *Pinus ponderosa* from contrasting climates. *Tree Physiology* 35: 535–548.

Kitajima, K., and J. A. Myers. 2008. Seedling ecophysiology: Strategies toward achievement of positive net carbon balance. *In* M. A. Leck, V. T. Parker, and R. L. Simpson [eds.], Seedling ecology and evolution, 172–188. Cambridge University Press, Cambridge, UK.

Kitin, P., Y. Sano, and R. Funada. 2003. Three-dimensional imaging and analysis of differentiating secondary xylem by confocal microscopy. *International Association of Wood Anatomists Journal* 24: 211–222.

Lambers, H., F. S. Chapin, and T. L. Pons. 2008. Plant physiological ecology, 2nd ed. Springer, New York, New York, USA.

Landis, T.D. 1989a. Irrigation and water management. *In* T. D. Landis, R. W. Tinus, S. E. McDonald, and J. P. Barnett [eds.], The container tree nursery manual, vol. 4, 68–118. Agriculture Handbook 674. U. S. Department of Agriculture, Forest Service, Washington, D.C., USA.

Landis, T.D. 1989b. Mineral nutrients and fertilization. *In* T. D. Landis, R. W. Tinus, S. E. McDonald, and J. P. Barnett [eds.], The container tree nursery manual, vol. 4, 1–67. Agriculture Handbook 674. U. S. Department of Agriculture, Forest Service, Washington, D.C., USA.

Lenth, R. V. 2016. Least-squares means: The R package lsmeans. *Journal of Statistical Software* 69: 1–32.

Maherali, H., B. L. Williams, K. N. Paige, and E. H. DeLucia. 2002. Hydraulic differentiation of ponderosa pine populations along a climate gradient is not associated with ecotypic divergence. *Functional Ecology* 16: 510–521.

Martínez-Vilalta, J., A. Sala, and J. Piñol. 2004. The hydraulic architecture of Pinaceae—A review. *Plant Ecology* 171: 3–13.

McCulloh, K. A., D. M. Johnson, F. C. Meinzer, and B. Lachenbruch. 2011. An annual pattern of native embolism in upper branches of four tall conifer species. *American Journal of Botany* 98: 1007–1015.

Melcher, P. J., N. M. Holbrook, M. J. Burns, M. A. Zwieniecki, A. R. Cobb, T. J. Brodribb, B. Choat, and L. Sack. 2012. Measurements of stem xylem hydraulic conductivity in the laboratory and field. *Methods in Ecology and Evolution* 3: 685–694.

Nolf, M., R. Lopez, J. M. R. Peters, R. J. Flabel, L. S. Koloadin, I. M. Young, and B. Choat. 2017. Visualization of xylem embolism by X-ray microtomography: A direct test against hydraulic measurements. *New Phytologist*.

Ogasa, M., N. H. Miki, Y. Murakami, and K. Yoshikawa. 2013. Recovery performance in xylem hydraulic conductivity is correlated with cavitation resistance for temperate deciduous tree species. *Tree Physiology* 33: 335–344.

Pallardy, S. G. 2008. Physiology of woody plants, 3rd ed. Elsevier, San Diego, California, USA.

Pérez-Harguindeguy, N., S. Díaz, E. Garnier, S. Lavorel, H. Poorter, P. Jaureguiberry, M. S. Bret-Harte, et al. 2013. New handbook for standardised measurement of plant functional traits worldwide. *Australian Journal of Botany* 61: 167–234.

Pfanz, H., G. Aschan, R. Langenfeld-Heyser, C. Wittmann, and M. Loose. 2002. Ecology and ecophysiology of tree stems: Corticular and wood photosynthesis. *Naturwissenschaften* 89: 147–162.

Piñol, J., and A. Sala. 2000. Ecological implications of xylem cavitation for several Pinaceae in the Pacific Northern USA. *Functional Ecology* 14: 538–545.

Pittermann, J., B. Choat, S. Jansen, S. A. Stuart, L. Lynn, and T. E. Dawson. 2010. The relationships between xylem safety and hydraulic efficiency in the Cupressaceae: The evolution of pit membrane form and function. *Plant Physiology* 153: 1919–1931.

Pittermann, J., J. S. Sperry, J. K. Wheeler, U. G. Hacke, and E. H. Sikkema. 2006a. Inter-tracheid pitting and the hydraulic efficiency of conifer wood: The role of tracheid allometry and cavitation protection. *American Journal of Botany* 93: 1265–1273.

Pittermann, J., J. S. Sperry, J. K. Wheeler, U. G. Hacke, and E. H. Sikkema. 2006b. Mechanical reinforcement against tracheid implosion compromises the hydraulic efficiency of conifer xylem. *Plant, Cell & Environment* 29: 1618–1628.

Preibisch, S., S. Saalfeld, and P. Tomancak. 2009. Globally optimal stitching of tiled 3D microscopic image acquisitions. *Bioinformatics* 25: 1463–1465.

Reich, P. B., I. J. Wright, J. Cavender-Bares, J. M. Craine, J. Oleksyn, M. Westoby, and M. B. Walters. 2003. The evolution of plant functional variation: Traits, spectra and strategies. *International Journal of Plant Sciences* 164(S3): S143–S164.

Reinhardt, K., M. J. Germino, L. M. Kueppers, J.-C. Domec, and J. Mitton. 2015. Linking carbon and water relations to drought-induced mortality in *Pinus flexilis* seedlings. *Tree Physiology* 35: 771–782.

Romberger, J. A., Z. Hejnowicz, and J. F. Hill. 2004. Plant structure: Function and development/A treatise on anatomy and vegetative development, with special reference to woody plants. Blackburn Press, Caldwell, New Jersey, USA.

RStudio Team. 2015. RStudio: Integrated development for R. RStudio, Boston, Massachusetts, USA. Website http://www.rstudio.com/.

Ruzin, S. E. 1999. Plant microtechnique and microscopy. Oxford University Press, New York, New York, USA.

Sant'Anna, C., L. T. Costa, Y. Abud, L. Biancatto, F. C. Miguens, and W. de Souza. 2013. Sugarcane cell wall structure and lignin distribution investigated by confocal and electron microscopy. *Microscopy Research and Technique* 76: 829–834.

Santiago, L. S., G. Goldstein, F. C. Meinzer, J. B. Fisher, K. Machado, D. Woodruff, and T. Jones. 2004. Leaf photosynthetic traits scale with hydraulic conductivity and wood density in Panamanian forest canopy trees. *Oecologia* 140: 543–550.

Schall, P., C. Lödige, M. Beck, and C. Ammer. 2012. Biomass allocation to roots and shoots is more sensitive to shade and drought in European beech than in Norway spruce seedlings. *Forest Ecology and Management* 266: 246–253.

Schindelin, J., I. Arganda-Carreras, and E. Frise. 2012. Fiji: An open source platform for biological-image analysis. *Nature Methods* 9: 676–682.

Schulte, P. J., U. G. Hacke, and A. L. Schoonmaker. 2015. Pit membrane structure is highly variable and accounts for a major resistance to water flow through tracheid pits in stems and roots of two boreal conifer species. *New Phytologist* 208: 102–113.

Simonin, K., T. E. Kolb, M. Montes-Helu, and G. W. Koch. 2006. Restoration thinning and influence of tree size and leaf area to sapwood area ratio on water relations of *Pinus ponderosa. Tree Physiology* 26: 493–503.

Spatz, H.-C., and K. J. Niklas. 2013. Modes of failure in tubular plant organs. *American Journal of Botany* 100: 332–336.

Sperry, J. S., U. G. Hacke, and J. Pittermann. 2006. Size and function in conifer tracheids and angiosperm vessels. *American Journal of Botany* 93: 1490–1500.

Sterck, F. J., J. Martínez-Vilalta, M. Menucuuini, H. Cochard, P. Gerrits, R. Zweifel, A. Herrero, et al. 2012. Understanding trait interactions and their impacts on growth in Scots pine branches across Europe. *Functional Ecology* 26: 541–549.

Stout, D. L., and A. Sala. 2003. Xylem vulnerability to cavitation in *Pseudotsuga menziesii* and *Pinus ponderosa* from contrasting habitats. *Tree Physiology* 23: 43–50.

Tyree, M. T., and F. W. Ewers. 1991. The hydraulic architecture of trees and other woody plants. *New Phytologist* 119: 345–360.

Tyree, M. T., and M. H. Zimmermann. 2002. Xylem structure and the ascent of sap, 2nd ed. Springer-Verlag, Heidelberg, Germany.

Urli, M., A. J. Porté, H. Cochard, Y. Guengant, R. Burlett, and S. Delzon. 2013. Xylem embolism threshold for catastrophic hydrualic failure in angiosperm trees. *Tree Physiology* 33: 672–683.

Venables, W. N., and B. D. Ripley. 2002. Modern applied statistics with S, 4th ed. Springer, New York, New York, USA.

Vertessy, R. A., R. G. Benyon, S. K. O'sullivan, and P. R. Gribben. 1995. Relationships between stem diameter, sapwood area, leaf area and transpiration in a young mountain ash forest. *Tree Physiology* 15: 559–567.

Zelinka, S. L., K. J. Bourne, J. C. Hermanson, S. V. Glass, A. Costa, and A. C. Wiedenhoeft. 2015. Force-displacement measurements of earlywood bordered pits using a mesomechanical tester. *Plant, Cell & Environment* 38: 2088–2097.

Zimmermann, M. H. 1983. Xylem structure and the ascent of sap. Springer-Verlag, Berlin, Germany.

Zuur, A. F., E. N. Ieno, N. J. Walker, A. A. Savelieve, and G. M. Smith. 2009. Mixed effects models and extensions in ecology with R. Springer, New York, New York, USA.